Computational Mechanics (2004) © Springer-Verlag 2004
DOI 10.1007/s00466-003-0546-9

On hexahedral finite element HC8/27 in elasticity

D. Mijuca

Abstract A new three-dimensional multifield finite element approach for analysis of isotropic and anisotropic materials in linear elastostatics, derived from primal–mixed variational formulation based on Hellinger-Reissner's principle, is presented. The novel properties are stress approximation by the continuous base functions, introduction of stress constraints as essential boundary conditions, and initial displacement and stress/strain field capability. It will be shown that resulting hexahedral finite element HC8/27 satisfies mathematical convergence requirements, like consistency and stability, even when it is rigorously slandered, distorted or used for the nearly incompressible materials. In order to minimise accuracy error and enable introductions of displacement and stress constraints, the tensorial character of the present finite element equations is fully respected. The proposed finite element is subjected to the number of standard pathological tests in order to test convergence of the results.

Keywords Finite elements, 3D problem, Multifield, Reliability, Elasticity, Geometric invariance

1 Introduction

The main objective of the present investigation is to develop a new hexahedral (brick) finite element that can reliably approximate behaviour of solid bodies of arbitrary geometry and material characteristics. The main motive is found in the possible need for the hexahedral finite elements that can reliably and simultaneously approximate displacements and stresses, even in the analysis of thin and thick solid bodies under the limit conditions. Further, the motive is also found in the known problem of connecting the finite elements of different dimensionality, i.e. when a model problem has geometrical transitions from solid to thick or thin. Consequently, present goal is to present hexahedral finite element that can approximate without locking solid body of arbitrary shape, of isotropic, orthotropic or anisotropic material, which is based on finite element approach that give us opportunity to introduce initial stress and/or strains.

For that purpose, let us remind that there are *single* and *multifield* finite element approaches, based on the canonical functional in the linear elastostatics. The most basic *single* field finite element approach in mechanics of solid body is based on the minimisation of the total potential energy functional. It is called displacement finite element method also, because displacement is only one master (primal) variable. It results with system matrix, which is positive definite, symmetric and sparse, thus enable us to use a number of efficient open codes for the solution of resulting system of linear equations. Further, it is easy to construct finite elements that satisfy mathematical convergence requirements – consistency and stability. However, it exhibits pathology in several limiting situations [1], as shear locking when low order elements are used, presence of spurious or kinematic modes (extra zero eigenvalues of system matrix) when selectively reduced integration is used, locking behaviour in problems involving internal constraints (e.g. incompressibility), as well as the finite element sensitivity to mesh distortion. In addition, stresses are calculated a posteriori, by differentiation over the finite element level, which resulting in unrealistic discontinuous stress picture with loss of accuracy. In addition, if for some reason we want to analyse thin solid bodies with solid finite elements based on this approach, it is usually not possible because of the locking effects.

On the other hand, a multifield method in computational mechanics is defined as one that has more than one primal (fundamental, master) field. If all fields of variables are of the same dimensionality the resulting multifield approach is called *mixed*, otherwise it is called *hybrid*.

The most frequent motivation for the use of mixed finite element methods is their robustness in the presence of above-mentioned limiting situations [1]. Nevertheless, from the reason that one has to deal with at least two fundamental variables, the overall stability of mixed approaches in elasticity is not easy to achieve [2, 3]. More clearly, in the elasticity, the first stability condition requires a large displacement approximation space in accordance to the stress approximation space, while the second stability condition requires a large stress approximation space in accordance to the one of the displacement.

Received: 27 January 2003 / Accepted: 5 December 2003
Published online: 20 January 2004

D. Mijuca
Department of Mechanics, Faculty of Mathematics,
University of Belgrade, Serbia and Montenegro
e-mail: dmijuca@matf.bg.ac.yu

This investigation is carried under the Grant IO1865 from Ministry of Science, Technology and Development of Republic of Serbia. The support is gratefully acknowledged. The author also would like to thank Professors Erkhard Ramm and Daya B Reddy for their valuable remarks.

Obviously, these two conditions are in contradiction. Consequently, the well balance between the approximation spaces of these two fundamental variables must be found in order to avoid instabilities [1, 2].

Nevertheless, there is a common opinion [1] that mixed methods have some serious drawbacks, like much more degrees of freedom than primal ones, indefinite system matrix, and spurious oscillations of dual variables in the presence of singularities. Further, some authors [2] comment: "...The use of C^0 discretization for the stress field should be avoided. The main reason for this is the difficulty in the numerical solution of the linear system of equations...".

The two most exploited multifield mixed variational formulations in the elastostatics are Hellinger-Reissner (displacements and stresses) [1] and Hu-Washizu (displacements, strains and stresses) formulations [4]. The Hellinger-Reissner functional is based on the complementary energy function, in which the constitutive laws need to be modified when the elements are used for non-linear materials. On the other hand, the Hu-Washizu functional is formulated in terms of strain energy function, thus making it more attractive for non-linear materials.

Another type of multifield variational principles are hybrid [5], where master fields are of different dimensionality, for example, one master field is volume and the other one is surface field. The main motive for their use is the relaxing of continuity condition on some field of interest to handle material interfaces, cracks or dislocations, as well as better displacement and stress solution in some limiting situations where single field approaches tends to be overstiff, like in above-mentioned situations.

Although there are many successful finite elements on the market, present investigation is oriented toward development of the general three-dimensional mixed finite element in elastostatics based on te Hellinger-Reissner's principle. It should be noted, that it is a continuation of the work in the settings of membrane elastostatics [6], where it was shown that present scheme is reliable, robust, and has superior performance in accordance to the raw displacement finite element method, on the fairly chosen set of standard benchmark examples.

Thus, the main properties of the present hexahedral finite element are:

1. stable and robust three-dimensional finite element HC8/27, insensitive to distortion and aspect ratio of its dimensions,
2. continuous displacement and stress fields, eliminating the need for stress recovering methods,
3. low-order approximation of displacements,
4. flexible hierarchic approximation of stresses, utilising from nine to twenty seven nodes per finite element, depending of the smoothness and regularity of the problem,
5. sparse indefinite symmetric system matrix,
6. calculations of displacements and stresses from the same system of algebraic equations by simple Gaussian elimination,
7. no spurious oscillations of stresses in the presence of singularity,
8. treatment of displacement and stress constrains as essential boundary conditions,
9. no numerical tricks or tune-ups, easy coding.

It should be noted that straightforward calculation of stresses is a great advantage from accuracy point of view [7] and avoidance of the stress recovery.

Nevertheless, in order to prevent occurring of *invariance error* [8], the geometric invariance of present governing equations is fully respected. In the present contribution, the proposed scheme is tested by the standard low and high order convergence tests, while the analysis of its efficiency is left for the future work.

2 Mixed problem

We will start from the primal-mixed weak form of the geometrically linear elastostatics field equations based on the Hellinger-Reissner's principle [1, 9, 10], that states:

$$\begin{aligned}
&\text{Find } \{\mathbf{u},\mathbf{T}\} \in H^1(\Omega)^n \times L^2(\Omega)^{n\times n}_{\text{sym}} \text{ such that} \\
&\quad \mathbf{u}|_{\partial\Omega_u} = \mathbf{w} \text{ and :} \\
&\int_\Omega (A\mathbf{T} : \mathbf{S} - \mathbf{S} : \nabla\mathbf{u} - \nabla\mathbf{v} : \mathbf{T})\,\mathrm{d}\Omega \\
&\quad = -\int_\Omega \mathbf{v}\cdot\mathbf{f}\,\mathrm{d}\Omega - \int_{\partial\Omega_t} \mathbf{v}\cdot\mathbf{p}\,\mathrm{d}\partial\Omega \\
&\qquad \text{for all } \{\mathbf{v},\mathbf{S}\} \in H^1(\Omega)^n \times L^2(\Omega)^{n\times n}_{\text{sym}} \\
&\qquad \text{such that } \mathbf{v}|_{\partial\Omega_t} = \mathbf{0}\ .
\end{aligned} \tag{1}$$

In the above formulation, $\mathbf{u}$ is the displacement field, $\mathbf{T}$ is the stress field, $\mathbf{f}$ is the vector of body forces and $\mathbf{p}$ is the vector of boundary tractions, $\mathbf{w}$ is the vector of prescribed displacements, while A is fourth order compliance tensor. Further, $\Omega \subset R^n$, $n = 1, 2, 3$ in an open bounded domain of the elastic body, where n is the number of spatial dimensions considered. Hence, $\mathbf{n}$ is the unit normal vector to the boundary $\partial\Omega$, while $\partial\Omega_u$ and $\partial\Omega_t$ are the portions of $\partial\Omega$ where the displacements or stresses are prescribed, respectively. The $\{\mathbf{u},\mathbf{T}\}$ and $\{\mathbf{v},\mathbf{S}\}$ are pairs of trial and test displacement and stress functions, respectively. As it could be seen, the stress functions are from discontinuous subspaces $L^2(\Omega)^{n\times n}_{\text{sym}}$, as in the case of the classical displacement method approach (see [1]). However, if there is no singularity or abrupt material change in the region of the model problem, it is a discrepancy from the reality which usually results in the lost of accuracy.

Accordingly, our present goal is to achieve full (three-dimensional) stress continuity. So, trial and test stress approximation functions are chosen from smaller but continuous finite element sub-space $H^1(\Omega)^{n\times n}_{\text{sym}}$, the space of all symmetric tensorfields that are square integrable and have square integrable gradients. It was already successfully used in [12] for linear triangles, and in [13] for bilinear isoparametric quadrilaterals. In both cases, numerical results have indicated high accuracy. The problem of solvability of such configurations has been elaborated in [14] by Zienkiewicz and Taylor et al. Further, to increase accuracy and to provide proper modelling of

the planes of symmetry, modelling of stress constraints as the essential boundary conditions was introduced in [15]. Moreover, stabilization of primal–mixed elements by full or partial hierarchic interpolation of stresses one order higher than displacements has been introduced in [16].

The detailed investigation of the present approach in two-dimensional (membrane) elasticity has proved that quadrilateral finite element QC4/9, with four corner displacement and nine stress nodes (four corner, four middle-sided and one central *bubble*), is more efficient than corresponding raw displacement method [7] and that it is reliable [16]. Only recently, present approach was extended to the three-dimensional case [17], where it has been shown that lowest-order finite element HC8/9 (eight displacement corner nodes, eight stress corner nodes and one *bubble* stress node) of that scheme is consistent, solvable, and satisfies the first stability condition. However, it does not satisfy second stability condition (inf–sup test), which was being expected because its two-dimensional counterpart QC4/5 does not pass that test [16], also.

2.1 Finite element spaces

Let C_h be the partitioning of the domain Ω into elements Ω_i and let us define the finite element subspaces for the displacement vector $\mathbf{u}$, the stress tensor $\mathbf{T}$ and the appropriate weight functions, respectively as:

$$\begin{aligned}
U_h &= \{\mathbf{u} \in (H^1)^n(\Omega) | \mathbf{u}|_{\partial\Omega_u} = \mathbf{w}, \mathbf{u}|_{\Omega_i} \\
&\quad = U^K(\Omega_i)\mathbf{u}_K, \Omega_i \in C_h\}, \\
V_h &= \{\mathbf{v} \in (H^1)^n(\Omega) | \mathbf{v}|_{\partial\Omega_u} = 0, \mathbf{v}|_{\Omega_i} \\
&\quad = V^K(\Omega_i)\mathbf{v}_K, \Omega_i \in C_h\}, \\
T_h &= \{\mathbf{T} \in (H^1)^{n\times n}(\Omega) | \mathbf{T}\cdot\mathbf{n}|_{\partial\Omega_t} = \mathbf{p}, \mathbf{T}|_{\Omega_i} \\
&\quad = T_L(\Omega_i)\mathbf{T}^L, \Omega_i \in C_h\}, \\
S_h &= \{\mathbf{S} \in (H^1)^{n\times n}(\Omega) | \mathbf{S}\cdot\mathbf{n}|_{\partial\Omega_t} = \mathbf{0}, \mathbf{S}|_{\partial\Omega_i} \\
&\quad = S_L(\Omega_i)\mathbf{S}^L, \Omega_i \in C_h\} \ .
\end{aligned}$$

In these expressions $\mathbf{u}_K$ and $\mathbf{T}^L$ are the nodal values of the displacement vector $\mathbf{u}$ and stress tensor $\mathbf{T}$ respectively. Accordingly, U^K and T_L are corresponding values of the interpolation functions, connecting displacements and stresses at an arbitrary point in Ω_i (the body of an element), and the nodal values of these quantities. The complete analogy holds for the displacement and stress variations (weight functions) $\mathbf{v}$ and $\mathbf{S}$, respectively.

To handle stress components adequately and conveniently, the boundary (interface) nodal coordinate surfaces should be accommodated to coincide or at least to tangent the local boundary surfaces and/or interfaces. In that case, it will be possible to treat known stress constraints as essential stress boundary conditions, also.

2.2 Numerical implementation

After discretization of the starting problem (2) by finite element method, it has been shown in [13] that present scheme can be written as the system of linear equations of order $n = n_u + n_t$, where n_u is the number of displacement degrees of freedom, while n_u is the number of stress degrees of freedom:

$$\begin{bmatrix} \mathbf{A}_{vv} & -\mathbf{D}_{vv} \\ -\mathbf{D}_{vv}^T & \mathbf{0} \end{bmatrix} \begin{bmatrix} \mathbf{t}_v \\ \mathbf{u}_v \end{bmatrix} = \begin{bmatrix} -\mathbf{A}_{vp} & \mathbf{D}_{vp} \\ \mathbf{D}_{pv}^T & \mathbf{0} \end{bmatrix} \begin{bmatrix} \mathbf{t}_p \\ \mathbf{u}_p \end{bmatrix} - \begin{bmatrix} \mathbf{0} \\ \mathbf{f}_p + \mathbf{p}_p \end{bmatrix} \ . \tag{2}$$

In this expression, unknown (variable) and known (initial, prescribed) values of the stresses and displacements, denoted by the indices v and p respectively, are decomposed. The nodal stresses t^{Lst} and displacements u_{Kq} components are consecutively ordered in the column matrices $\mathbf{t}$ and $\mathbf{u}$ respectively. The homogeneous (zero) and nonhomogenous (nonzero) essential boundary conditions per displacements $\mathbf{u}_p$ and stresses $\mathbf{t}_p$ are introduced as contribution to the right-hand side of the expression (2).

The members of the matrices $\mathbf{A}$ and $\mathbf{D}$, of the column matrices $\mathbf{f}$ and $\mathbf{p}$ (discretized body and surface forces) in (2), are respectively:

$$A_{\Lambda u v \Gamma s t} = \sum_e \int_{\Omega_i} \Omega^N_\Lambda S_N g^a_{(\Lambda)u} g^b_{(\Lambda)v} A_{abcd} g^c_{(\Gamma)s} g^d_{(\Gamma)t} T_L \Omega^L_\Gamma \ \mathrm{d}\Omega \ , \tag{3}$$

$$D^{\Gamma q}_{\Lambda u v} = \sum_e \int_{\Omega_i} \Omega^N_\Lambda S_N U^K_a \Omega^\Gamma_K g^a_{(\Lambda)u} g^{(\Gamma)q}_{(\Lambda)v} \ \mathrm{d}\Omega \ , \tag{4}$$

$$f^{\Lambda q} = \sum_e \int_{\Omega_i} g^{(\Lambda)q}_a \Omega^\Lambda_M V^M f^a \ \mathrm{d}\Omega \ , \tag{5}$$

$$p^{\Lambda q} = \sum_e \int_{\partial\Omega_{it}} g^{(\Lambda)q}_a \Omega^\Lambda_M V^M p^a \ \mathrm{d}\partial\Omega \ . \tag{6}$$

The use of indices is taken from [18]. So, in the above expressions $z^i(i,j,k,l = 1,2,3)$ is the Cartesian coordinate system of the whole model problem, that is global coordinate system of the model. Further, $x^{(K)n}(m,n,p,q = 1,2,3)$ and $y^{(K)s}(r,s,t,u,v = 1,2,3)$ are displacement and stress coordinate systems at each global node K, respectively, not necessarily of the same position and kind. Possibility to choose different coordinate systems at the global nodes per displacements and stresses will enable us to select proper positions of nodal coordinate systems for introduction of stress and displacement constraints.

The local natural (convective) coordinate systems per finite elements are denoted by $\xi^a(a,b,c,d = 1,2,3)$. While, $g^{(K)mn}$ and g^{ab} are the components of the contravariant fundamental metric tensors, the first one with respect to $x^{(K)n}$ at global node K (i.e. Λ), and the second to ξ natural coordinate system of a finite element. Furthermore, $U^K_a = \partial U^K / \partial \xi^a$.

Also, A_{abcd} are the components of the elastic fourth order compliance tensor. In the case of isotropic material,

in order to determine compliance matrix with six independent components we will need to know Young's modulus and Poisson's ratio, only. Further, in the case of orthotropic material we will need to know Young's modulus E_1, E_2 and E_3 in each of three mutually perpendicular directions called the principal directions, six Poisson's ratio v_{12}, v_{13}, v_{23}, v_{21}, v_{31}, v_{32}, as well as three shear moduli G_{12}, G_{13} and G_{23}, from which we will calculate compliance matrix. On the other hand, in the case of anisotropic materials, in the most general case, we will need to know 21 independent coefficients of the compliance matrix. Further, f^a and p^a are the body forces and boundary tractions in natural coordinates of an element, respectively.

Integration is performed over the domain Ω_i of each element, or where the tractions are given over the part of the boundary surface $\partial\Omega_{it}$, while summation is over all the **e** elements of a system.

In the end, Ω_K^Λ is a connectivity operator (see [18], p. 26), which maps the set of global nodes Λ into the set of local nodes K per elements, and vice versa. Next, the upper case letters in parentheses give us information to which node, local per element, or equivalently, global per model, considered quantity is related. Let us explain the need for the connectivity operator from the aspect of actual coding of the present scheme. The assembling of all entries in (4) is performed per elements (**e**) and local nodes in these elements (K), in the local natural coordinate systems (ξ^a). On the other hand, input quantities (boundary conditions, external forces, etc.) are given per global coordinate systems in global nodes (x^i – displacements and forces, y^i – stresses). Therefore, we need the connectivity operator

$$[\mathbf{A}] = \begin{bmatrix} \frac{1}{E_1} & -\frac{v_{21}}{E_2} & -\frac{v_{31}}{E_3} & 0 & 0 & 0 \\ -\frac{v_{12}}{E_1} & \frac{1}{E_2} & -\frac{v_{32}}{E_3} & 0 & 0 & 0 \\ -\frac{v_{13}}{E_1} & -\frac{v_{23}}{E_2} & \frac{1}{E_3} & 0 & 0 & 0 \\ 0 & 0 & 0 & \frac{1}{G_{12}} & 0 & 0 \\ 0 & 0 & 0 & 0 & \frac{1}{G_{13}} & 0 \\ 0 & 0 & 0 & 0 & 0 & \frac{1}{G_{23}} \end{bmatrix}, \tag{8}$$

The Euclidean shifting operators $g^{(K)m}_{(L)s}$, $g^a_{(L)s}$ and $g^{(K)q}_b$ are, respectively:

$$g^{(K)m}_{(L)s} = \delta_{kl} g^{(K)mn} \frac{\partial z^k}{\partial x^{(K)n}} \frac{\partial z^l}{\partial y^{(L)s}} \ , \tag{9}$$

$$\begin{aligned} g^a_{(L)s} &= \delta_{kl} g^{ab} \frac{\partial z^k}{\partial \xi^b} \frac{\partial z^l}{\partial y^{(L)s}}, \\ g^{(K)q}_b &= \delta_{kl} g^{(K)qp} \frac{\partial z^k}{\partial \xi^b} \frac{\partial z^l}{\partial x^{(K)p}} \ . \end{aligned} \tag{10}$$

For the reason that tensorial character is fully respected, one can easily choose appropriate coordinate system at each global node for the introductions of known stresses and/or displacements, or interpretation of the results.

2.3
Some details on the solution procedure

For the sake of the better insight in the solution procedure, the system matrix entries in (2) will be examined. For each mutually interconnected (by the common element(s)) pair of nodes L and M, or L and K, respectively, submatrices of A and D have following structure, respectively:

$$[A_{LM}] = \begin{bmatrix} A_{L11M11} & A_{L11M22} & A_{L11M33} & A_{L11M12}+A_{L11M21} & A_{L11M13}+A_{L11M31} & A_{L11M23}+A_{L11M32} \\ A_{L22M11} & A_{L22M22} & A_{L22M33} & A_{L22M12}+A_{L22M21} & A_{L22M13}+A_{L22M31} & A_{L22M23}+A_{L22M32} \\ A_{L33M11} & A_{L33M22} & A_{L33M33} & A_{L33M12}+A_{L33M21} & A_{L33M13}+A_{L33M31} & A_{L33M23}+A_{L33M32} \\ A_{L12M11}+A_{L21M11} & A_{L12M22}+A_{L21M22} & A_{L12M33}+A_{L21M33} & \begin{matrix} A_{L12M12}+A_{L12M21}+ \\ A_{L21M12}+A_{L21M21} \end{matrix} & \begin{matrix} A_{L12M13}+A_{L12M31}+ \\ A_{L21M13}+A_{L21M31} \end{matrix} & \begin{matrix} A_{L12M23}+A_{L12M32}+ \\ A_{L21M23}+A_{L21M32} \end{matrix} \\ A_{L13M11}+A_{L31M11} & A_{L13M22}+A_{L31M22} & A_{L13M33}+A_{L31M33} & \begin{matrix} A_{L13M12}+A_{L13M21}+ \\ A_{L31M12}+A_{L31M21} \end{matrix} & \begin{matrix} A_{L13M13}+A_{L13M31}+ \\ A_{L31M13}+A_{L31M31} \end{matrix} & \begin{matrix} A_{L13M23}+A_{L13M32}+ \\ A_{L31M23}+A_{L31M32} \end{matrix} \\ A_{L23M11}+A_{L32M11} & A_{L23M22}+A_{L32M22} & A_{L23M33}+A_{L32M33} & \begin{matrix} A_{L23M12}+A_{L23M21}+ \\ A_{L32M12}+A_{L32M21} \end{matrix} & \begin{matrix} A_{L23M13}+A_{L23M31}+ \\ A_{L32M13}+A_{L32M31} \end{matrix} & \begin{matrix} A_{L23M23}+A_{L23M32}+ \\ A_{L32M23}+A_{L32M32} \end{matrix} \end{bmatrix} \tag{11}$$

which will give us information to which element considered global node Λ belongs, and which local number it has in that element. The transformations of the considered tensorial quantity in that global node, from the coordinate system in nodes (x^i or y^i) to natural local coordinate systems (ξ^a) is done by the use of the Euclidian shifters $(g^a_{(\Lambda)u})$. All entries in (2) are presently calculated by using a $3 \times 3 \times 3$ Gaussian integration formula.

Hence, the coefficients of the fourth-order compliance tensor A_{abcd} in the general three-dimensional analysis of isotropic material are calculated by:

$$A_{abcd} = \frac{1}{2E}[(1+v)(g_{ca}g_{db} + g_{cb}g_{da}) - 2v g_{ab}g_{cd}] \ . \tag{7}$$

While, for orthotropic material we have compliance matrix in form:

$$[D^{Kq}_{Lst}] = \begin{bmatrix} D^{K1}_{L11} & D^{K2}_{L11} & D^{K3}_{L11} \\ D^{K1}_{L22} & D^{K2}_{L22} & D^{K3}_{L22} \\ D^{K1}_{L33} & D^{K2}_{L33} & D^{K3}_{L33} \\ D^{K1}_{L12}+D^{K1}_{L21} & D^{K2}_{L12}+D^{K2}_{L21} & D^{K3}_{L12}+D^{K3}_{L21} \\ D^{K1}_{L13}+D^{K1}_{L31} & D^{K2}_{L13}+D^{K2}_{L31} & D^{K3}_{L13}+D^{K3}_{L31} \\ D^{K1}_{L23}+D^{K1}_{L32} & D^{K2}_{L23}+D^{K2}_{L32} & D^{K3}_{L23}+D^{K3}_{L32} \end{bmatrix} \tag{12}$$

While, stress and displacement components are presently ordered in the following way $[t^T] = [t^{11}, t^{22}, t^{33}, t^{12}, t^{13}, t^{23}]$ and $[u^T] = [u^1, u^2, u^3]$, respectively. So, vector of unknown values or vector of prescribed (initial) values is $[t^{11}, t^{22}, t^{33}, t^{12}, t^{13}, t^{23}, u^1, u^2, u^3]$. In these expressions indices 1, 2 and 3 correspond to the components of

displacement vector at the node K, while the indices 11, 22, 33, 12, 13 and 23 correspond to the components of symmetric stress tensor at nodes L and/or K.

The first main programming step in the above problem is an assembly procedure of the left and right sides of (2). The second one is the solution procedure of the resulting system (2). The most natural and the fastest way in the assembly procedure is to loop through the elements, by putting in connection pairs of nodes L and M. At the left side of (2), the unconstrained degrees of freedom (components t_v and u_v) connected with the current node L are retained. At the right side, the terms connected with the known components t_p and u_p are situated. The rows and columns connected with the components with zero t_p and u_p are neglected.

The matrix on the left side of (2) is indefinite, symmetric and sparse. Presently, for the solution the symmetric sparse Gaussian elimination procedure is used. It should be noted that zeroes at the main diagonal of the system matrix are not an obstacle, because triangularization procedure fills these positions with nonzero values.

2.4
Finite element HC8/27

The finite element HC8/27 is shown in Fig. 1. Its acronym is taken from [14], where the first letter H stands for hexahedral element geometrical shape, while the letter C indicates the use of continuous approximation functions. The displacement nodes are denoted by spheres, while stress nodes are denoted by tetrahedrons, as shown in Fig. 1.

The displacement field is approximated by tre–linear shape functions, connected to eight corner nodes numbered from 1–8. On the other hand, nodes from eight to twenty-seven are used for the approximation of the stress field. Beside eight basic stress corner nodes, stabilization of finite element is achieved by full or partial hierarchic interpolation of stresses one order higher than displacements connected to the additional nineteen stress nodes. Thus, twenty-seven stress nodes are used to accommodate full triquadratic expansion in natural coordinates ξ, η and ζ. From these, eight stress corner nodes are connected to the tre-linear shape functions denoted from 1–8. Further, eleven quadratic shape functions are connected to the midpoints of the sides numbered from 9–20. Six

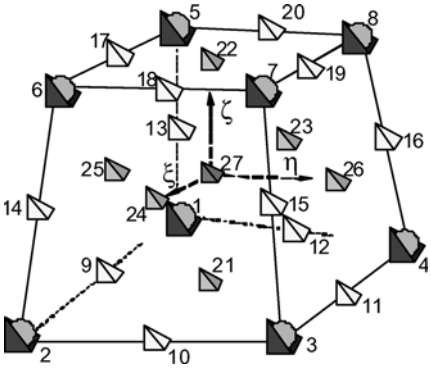

Fig. 1. Finite element HC8/27

biquadratic stress shape functions are connected to each face centre, numbered from 21–26, and one three-quadratic shape function connected to the hexahedron centre (*bubble* node) numbered by 27. Consequently, multi-field combination of eight displacement and eight stress nodes is called HC8/8. The same basic element with additional one or nineteen stress nodes, is called HC8/9 or HC8/27, respectively. Further, per each node there are three displacement and six stress degrees of freedom. Consequently, there are maximum 186 degrees of freedom per one finite element (finite element HC8/27). In the case when analysed model problem is compressible and/or boundary conditions are smooth, we will use only 78 degrees of freedom (finite element HC8/9).

It should be noted, that from the point of view of actual coding, the coarser finite elements HC8/8 and HC8/9 are seen as finite element HC8/27, where degrees of freedom connected to the unwanted nodes are neglected (set to zero).

The element considered here can be in fact identified as an application of the Taylor-Hood type element in elasticity, for which Brezzi et al. [2] at p. 284 in example 3.3, have said: "It is not known if this element is stable".

2.5
On the construction of solvable and stable configurations

For forming the stable primal–mixed system of algebraic equations, the solvability and stability analyses (See Sects. 3 and 4) are taken into account. If there are no traction boundary conditions imposed (i.e. no essential boundary conditions per stresses) isoparametric finite element HC8/8 is used, which is sufficient to maintain the solvability of a system (see Table 1).

On the other hand, when essential traction boundary conditions are introduced, on the boundary and especially in corner elements, mechanisms can develop. In that case, it is necessary to add a central, bubble (HC8/9), node and some or all additional 18 quadratic nodes (HC8/27), not necessarily in all elements, to ensure solvability. Practically, the additional 1–18 second order stress nodes are hierarchic, that is the local approximation functions connected to these nodes are hierarchic. Nevertheless, any of these nodes can be added or suppressed using the simple technique equivalent to the definition of the boundary conditions.

The FORTRAN program code upon the full configuration of the finite element HC8/27 is written. However, if we want to analyse our model problem with *simpler* finite elements HC8/8 or HC8/9, we will simply set to zero all degrees of freedom connected to the unwanted hierarchic nodes.

Nevertheless, the results of inf–sup test (see Sect. 5) show that solvable configurations are not automatically stable. Further, more efficient solution procedure is obtained when nested dissection [7, 19] ordering of nodes is adopted.

3
Low order tests

In order to check necessary and sufficient conditions for convergence, as well as to check capability to represent

Table 1. Eigenvalues for different one finite element configurations

Mode (dof)	dof	H1/ME9 $\nu = 0.49999$ Undistorted	HC8/8 $\nu = 0.3$ Undistorted	HC8/9 $\nu = 0.3$ Undistorted	HC8/9 $\nu = 0.49999$ Undistorted	HC8/27 $\nu = 0.3$ Undistorted	HC8/27 $\nu = 0.49999$ Undistorted	HC8/27 $\nu = 0.49999$ Distorted
1	Displacement	∞	−0.2266E+00	−0.2821E+00	−0.3262E+00	−0.4855E+00	−0.6490E+00	−0.7010E+00
2		0.3333E+00	−0.2266E+00	−0.2497E+00	−0.2307E+00	−0.3099E+00	−0.2773E+00	−0.3440E+00
3		0.3333E+00	−0.2266E+00	−0.2497E+00	−0.2307E+00	−0.3099E+00	−0.2773E+00	−0.3386E+00
4		0.3333E+00	−0.2262E+00	−0.2497E+00	−0.2307E+00	−0.3099E+00	−0.2773E+00	−0.2693E+00
5		0.3333E+00	−0.1816E+00	−0.2077E+00	−0.1952E+00	−0.2807E+00	−0.2545E+00	−0.2451E+00
6		0.3333E+00	−0.1816E+00	−0.2077E+00	−0.1952E+00	−0.2807E+00	−0.2545E+00	−0.2213E+00
7		0.3333E+00	−0.1211E+00	−0.1211E+00	−0.1155E+00	−0.1689E+00	−0.1614E+00	−0.1863E+00
8		0.3333E+00	−0.9266E−01	−0.9266E−01	−0.9500E−01	−0.1457E+00	−0.1614E+00	−0.1790E+00
9		0.3333E+00	−0.9266E−01	−0.9266E−01	−0.9500E−01	−0.1457E+00	−0.1614E+00	−0.1688E+00
10		0.2222E+00	−0.9266E−01	−0.9266E−01	−0.9500E−01	−0.1457E+00	−0.1557E+00	−0.1348E+00
11		0.1111E+00	−0.8553E−01	−0.8553E−01	−0.8174E−01	−0.1211E+00	−0.1120E+00	−0.1289E+00
12		0.1111E+00	−0.8553E−01	−0.8553E−01	−0.8174E−01	−0.1211E+00	−0.1120E+00	−0.1147E+00
13		0.1111E+00	−0.8553E−01	−0.8553E−01	−0.8174E−01	−0.1211E+00	−0.1120E+00	−0.1071E+00
14		0.5556E−01	−0.4522E−01	−0.4522E−01	−0.4167E−01	−0.5327E−01	−0.4759E−01	−0.5784E−01
15		0.5556E−01	−0.4522E−01	−0.4522E−01	−0.4167E−01	−0.5327E−01	−0.4759E−01	−0.5281E−01
16		0.5556E−01	−0.3669E−01	−0.3669E−01	−0.3604E−01	−0.4557E−01	−0.4504E−01	−0.4725E−01
17		0.5556E−01	−0.3669E−01	−0.3669E−01	−0.3604E−01	−0.4557E−01	−0.4504E−01	−0.4553E−01
18		0.5556E−01	−0.3669E−01	−0.3669E−01	−0.3604E−01	−0.4557E−01	−0.4504E−01	−0.4297E−01
19–24	zero	0	0	0	0	0	0	0
25	stress		0.1852E−02	0.1852E−02	0.9259E−07	0.3638E−03	0.1819E−08	0.1819E−08
26–71			–	–	–	–	–	–
72			0.5516E−00	–	–	–	–	–
26–77				–	–	–	–	–
78				0.8740E+00	0.9517E+00	–	–	–
79–187						–	–	–
188						0.2808E+01	0.3161E+01	0.3317E+01

rigid body modes and constant strain condition, the low order tests are traditionally the first steps in the validation process of any new finite element. In addition, some authors considered these tests as tools for assessment of robustness of finite element algorithms. In the present paper the necessary [14] and sufficient conditions for solvability [20, 21] tests, are considered.

3.1
Necessary conditions for solvability

It is considered that single finite element passes solvability test, if the number of its stress degrees of freedom n_t is greater than number of displacement degrees of freedom n_u. This test is known [14] as single element patch test.

In the case of present finite element HC8/27 we have $n_u = 24$ and $n_t = 162$. So evidently, it passes the present test. In addition, its simpler configurations, HC8/8 and HC8/9, pass the present test also, because $n_t^{HC8/8} = 48$ and $n_t^{HC8/9} = 54$, that are again greater than the number of the displacements degrees of freedom $n_u = 24$.

3.2
Sufficient conditions for solvability. Eigenvalue analysis

In order to check if one finite element is sensitive to the locking phenomena, that is, to illustrate that element is free of spurious zero-energy modes (*mechanisms*), an eigenvalue analysis of single finite element is usually performed [21]. This test is also known as sufficient conditions for solvability test. It should be noted that one finite element free of boundary conditions, passes sufficient solvability test if the number of zero eigenvalues of the relevant system matrix in Eq. (2) is equal to the number of the rigid body modes. In the three-dimensional case, that number is six. If it is greater than six, some mechanisms are present and the problem is not solvable. In that case, the finite element will exhibit an apparent strain without any stress [20].

For the present finite element HC8/27, the number of negative eigenvalues corresponds to the number of displacement degrees of freedom ($n_u = 8 \times 3 = 24$), while the number of positive eigenvalues corresponds to the number of stress degrees of freedom ($n_t = 27 \times 6 = 162$). In addition, for a locking free element, only one mode corresponding to the dilatational mode should tend toward infinity in the limit of incompressibility or extreme aspect ratio. If any of additional modes tend toward infinity, the element will exhibit volumetric locking.

The test was performed over the undistorted or distorted one finite element configuration (see Fig. 2), where Young's modulus is $E = 1$ and Poisson's ratio is $\nu = 0.3$ or $\nu = 0.49999$. No displacement or stress boundary conditions were applied. The finite element H1/ME9 based on the mixed-enhanced strain method with nine enhanced modes [21] that passes present test in the nearly incompressible case, was taken for comparison.

In the Table 1, calculated eigenvalues are sorted in increasing order. All eigenvalues connected to the displacement degrees of freedom are reported. On the other hand, only the first and last eigenvalues connected to stress degrees of freedom are reported here. For example, one may see that finite element H1/ME9 has 24 eigenvalues connected to displacement degrees of freedom, from which six zero degrees of freedom are connected to rigid body modes. On the other hand, finite element HC8/27 has

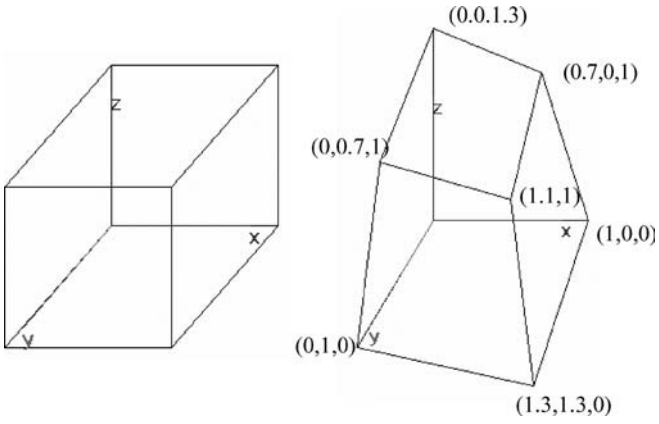

Fig. 2. Undistorted and distorted FE configurations

24 eigenvalues connected to displacement degrees of freedom, from which 6 zero degrees of freedom are connected to rigid body modes, and 162 positive eigenvalues connected to stress degrees of freedom. Therefore, for that element, all 18 negative eigenvalues connected to displacement degrees of freedom are listed, 6 zero degrees of freedom are shown in one raw, and finally from 162 eigenvalues connected to stress degrees of freedom, only the first (minimum) and last (maximum) are shown.

We may see that present hexahedral finite elements HC8/8, HC8/9 and HC8/27, pass the present test, regardless of the value of Poisson's ratio or the aspect ratio of theirs axial maximal dimensions.

4
The mathematical convergence requirements

As the finite element mesh is refined, the solution of discrete problem should approach to the analytical solution of the mathematical model, i.e. to converge. The convergence requirements for shape functions of isoparametric element can be grouped into three categories, that is: completeness, compatibility and stability [1, 11]. Consequently, we may say that consistency and stability imply convergence.

Completeness criterion requires that elements must have enough approximation power to capture the analytical solution in the limit of a mesh refinement process. Therefore, the finite element approximation functions must be of a certain polynomial order ensuring that all integrals in the corresponding weak formulation are finite. Specifically, if m is variational index calculated as the highest spatial derivative order that appears in the energy functional of the relevant boundary value problem, than the element base approximation functions must represent exactly all polynomial terms in order $\leq m$ in element coordinate system. A set of shape functions that satisfies this condition is called m-complete.

Further, *compatibility* criterion requires that finite element shape functions should provide displacement continuity between elements, in order to provide that no artificial material gaps will appear during the deformation. As the mesh is refined, such gaps could multiply and may absorb or release spurious energy. So, patch trial functions must be C^{m-1} continuous between interconnected elements, and C^m piecewise differentiable inside each element.

Nevertheless, completeness and compatibility are two aspects of the so-called *consistency* condition between the discrete and mathematical models. A finite element model that passes both, completeness and continuity requirements, is called *consistent*.

Further, if the considered finite element is *stable*, the non-physical zero-energy modes (kinematic modes) in finite element model problem will be prevented. The overall stability of mixed formulations based on Hellinger-Reissner's principle, is provided if two necessary conditions for stability are fulfilled i.e., the first condition represented by the *ellipticity on the kernel* condition and second condition represented by the *inf-sup* condition [1, 11].

It should be noted that satisfaction of the completeness criterion is necessary for the convergence, while violating other two criteria does necessary mean that solution will not converge.

4.1
Consistency condition

Presently, variational indices for displacement variable field and stress variable filed are both $m = 1$. Further, in the present formulation test and trial displacement approximation functions are from the space $H^1(\Omega)^n$, the space of all vectorfields that are square integrable and have square integrable gradients. Consequently, they are chosen to have C^0 continuity, represented by tre–linear polynomial functions. Accordingly, the completeness and compatibility requirements for that field are satisfied in the present case. Further, same conclusion is valid for the stress field also. Although, from the reason that stress derivatives do not appear in the present formulation, the continuity requirement on the trial and test stress shape functions may be relaxed to be C^{-1} (discontinuous) between the elements and C^0 inside, which will be exploited in the future investigations to analyse singularities and abrupt material changes.

4.2
First stability condition

The *ellipticity on the kernel* condition [1] is given by:

$$a(z,z) \leq \alpha_h \|z\| \quad \text{for all } z \in Z_h,$$
$$Z_h = \{z \in S_h | b(z,v) = 0 \text{ for all } v \in V_h\} \ , \quad (13)$$

where S_h and V_h are stress and displacement test approximation functions respectively. It should be noted that presently, test and trial stress local approximation functions are from continuous finite element subspaces $S_h \subset (H^1)^{n\times n}$. Therefore, the corresponding bilinear form a in (13) is quadratic. In addition, in the physical sense it represents the deformation energy that is positive definite in linear elasticity. Consequently, form a is symmetric and bounded, also.

On the other hand, the first stability condition could be evaluated using the matrix notation, also. The first equation in (2) will be well posed if:

$$\mathbf{s}^T \mathbf{A} \mathbf{s} \geq \alpha \|\mathbf{s}\|^2 \ . \quad (14)$$

Presently, the natural stress norm is also an energy norm, thus:

$$\frac{\mathbf{s}^T\mathbf{A}\mathbf{s}}{\|\mathbf{s}\|^2} = \frac{\mathbf{s}^T\mathbf{A}\mathbf{s}}{\mathbf{s}^T\mathbf{A}\mathbf{s}} = 1 \quad \Rightarrow \quad \alpha = 1 > 0 \tag{15}$$

Hence, for the present formulation, the first stability condition is satisfied a priori.

4.3
Second stability condition

For the presently investigated finite element, the second stability condition is satisfied if value γ_h, following from LBB (Ladyzhenskaya, Babuška, Brezzi) condition (see [5], p. 76, Eq. (3.22)), remains bounded above zero for the meshes of increasing density:

$$\gamma \le \gamma_h = \inf_{v \in H^{1(n)}} \sup_{\mathbf{S} \in H^{1(n\times n)}} \frac{b(\mathbf{S}_h, v_h)}{\|\mathbf{S}_h\| \|\mathbf{v}_h\|} \ , \tag{16}$$

where:

$$b(\mathbf{S}_h, \mathbf{v}_h) = \sum_e \int_{\Omega_i} \mathbf{S}_h : \nabla \mathbf{v}_h \ \mathrm{d}\Omega_e \ , \tag{17}$$

$$\|\mathbf{S}_h\|^2 = \sum_e \int_{\Omega_i} \mathbf{S}_h : \mathbf{S}_h \ \mathrm{d}\Omega_e \ , \tag{18}$$

$$\|\mathbf{v}_h\|^2 = \sum_e \int_{\Omega_i} \nabla \mathbf{v}_h^{\mathrm{T}} : \nabla \mathbf{v}_h \ \mathrm{d}\Omega_e \ . \tag{19}$$

In addition, condition (16) ensures solvability and optimality of the finite element solution [11]. It should be emphasized also, that any loading does not enter the present test.

Because verification of the condition like (16) involves an infinite number of meshes, it can not be performed. Therefore, numerical inf–sup [11] test should be performed for a sequence of meshes of increasing refinement. Consequently, in the present case, numerical *inf–sup* test is represented by generalized eigenvalue problem, in matrix notation given by:

$$\mathbf{D}_h^{\mathrm{T}} \mathbf{A}^{-1} \mathbf{D}_h \mathbf{x} = \lambda \mathbf{K}_h \mathbf{x} \ , \tag{20}$$

where **D** and **A** are matrix entries in (2). Further, matrix **K** is the stiffness matrix from the corresponding displacement finite element method, where entries are given by:

$$K^{\Lambda m \Gamma n} = \sum_e \Omega_L^{\Lambda} \int_{\Omega_i} g_a^{(\Lambda)m} U_b^L C^{abcd} U_d^K g_c^{(\Gamma)n} \ \mathrm{d}\Omega\Omega_K^{\Gamma}. \tag{21}$$

In the above expression, the fourth order elasticity tensor C^{abcd} in general three-dimensional analysis of isotropic materials is given by:

$$C^{abcd} = \frac{Ev}{(1+v)(1-2v)} g^{ab} g^{cd} + \frac{E}{2(1+v)} (g^{ac} g^{bd} + g^{ad} g^{bc}) \ . \tag{22}$$

The square root of the smallest eigenvalue of the problem (20), that is $\sqrt{\lambda_{\min}}$, is equal to the inf–sup value γ_h in (16).

If the inf–sup values, for chosen sequence of finite element meshes, do not show decrease toward zero (meaning that the $\lambda_{\min}$ values stabilize at some positive level) it can be said that inf–sup test is passed. It should be noted that decreasing of the inf–sup values on log-log diagram would be seen as curve with moderate or excessive slope. This approach was already used in [16] for testing the stability of quadrilateral finite elements QC4/5 and QC4/9, and in [17] for testing the stability of the hexahedral finite element HC8/9.

5
Inf–sup numerical test

In the present chapter, we will investigate if the present finite element HC8/27 passes numerical inf–sup test (20). It is suggested in [3, 11] to test the finite elements in different scenarios, such as: distorted or irregular finite element meshes, small thickness, bending and membrane dominated situations, and increasing Poisson's ratio toward incompressibility.

The results are plotted in the form $\log(\lambda_{\min}) = f(1/N)$, where $N = 1, \ldots, 8$ is the number of elements per side, while $\lambda_{\min}$ is the minimal eigenvalue in (20), where results for meshes of increasing refinement are plotted from right to left.

5.1
Membrane dominated case

As an example of membrane dominated case, the cylinder model problem with clamped edges is analysed [3]. The cylinder radius is $r = 1$, the full length is $L = 2$. To explore the sensitivity of the present hexahedral finite element HC8/27 to the values of thickness t in radial direction, two cases $t = 1/50$ and $t = 1/100$, are considered. The Young's modulus is $E = 1$, and Poisson's ratio is $v = 0.3$.

Because of symmetry, only one eight of the starting model problem, shown in Fig. 3, is considered. Further, one layer of finite elements is placed along the thickness. The finite element models for mesh indicator $N = 2, 4, 6, 8$ are considered. Total number of degrees of freedom (dof) per each of the mesh made from HC8/9 finite elements, is

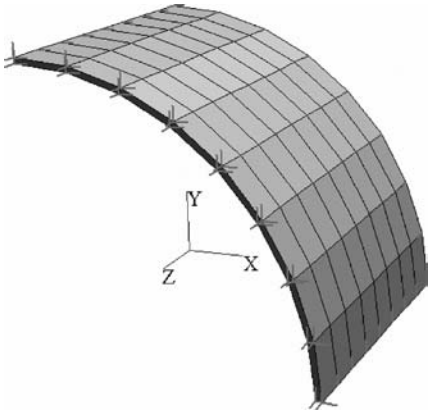

Fig. 3. Clamped cylinder: undeformed configurations $8 \times 8 \times 1$

dof $= 142, 470, 990, 1702$, while for the HC8/27 meshes we have dof $= 442, 1498, 3178, 5482$.

From the Fig. 4, we may see that regardless of the thickness, curves for the finite element HC8/9 have excessive slope, so that element does not pass inf–sup test. On the other hand, curves for finite element HC8/27 in either case of thickness, do not show decrease toward zero as the mesh is refined. Moreover, these curves are almost identical. Therefore, we may conclude that finite element HC8/27 passes inf–sup test in membrane dominated cases regardless of the considered thickness.

5.2
Bending dominated case

In order to investigate if the present finite element passes inf–sup test in the bending dominated situations [11], a clamped thin square model problem under the transverse uniform load $q = 1$, side $a = 2$ and thickness $t = 0.01$, is considered,. The Young's modulus is $E = 1$, and Poisson's ratio is $v = 0.3$. Only a quarter of the plate is analysed due to its overall symmetry, by the sequence ($N \times N \times 1$, $N = 2, 4, 6, 8, 10$) of undistorted meshes or the sequence of the highly distorted meshes that are not similar to each other. The stress boundary conditions are introduced as essential, which means that stresses $t^{zz}|_{t=0.01} = -1$ at the top surface of the plate are prescribed. The highly distorted finite element model $10 \times 10 \times 1$, is shown in Fig. 5, while other finite element meshes are shown in Fig. 6.

From the results shown in Fig. 6, it is evident that finite element HC8/27 passes inf–sup test in the case of bending dominated problems regardless of the level of distortion of the finite element mesh, since minimal generalised eigenvalues of the numerical inf–sup test problem (20) stabilise in the mesh refinement process. Therefore, we may say that the present finite element is robust in accordance to the level of the mesh distortion.

5.3
Near incompressibility case

On the model problem of the square block $(a = 2)$ under tri-axial tension, we will examine if the present finite element passes inf–sup test in the near incompressible scenario. Only one-eight of the starting model can be discretized due to the symmetry. Four finite element configurations with the mesh indicator $N = 1, 2, 3, 4$, are considered. Both, the displacement and stress boundary conditions are prescribed to simulate tri-axial tension, expect for the case with Poisson's ratio $v = 0.49$, where only displacements boundary conditions are prescribed.

From the Fig. 7, it may be seen that the smallest non-zero eigenvalues stabilize after one-element configuration, similar as in [3] for MITC finite element family. Therefore, we may conclude that finite element HC8/27 passes inf–sup test in compressible and nearly incompressible cases.

6
Numerical examples

In order to check the convergence of the present formulation, the number of challenging benchmark tests were performed, using the finite element HC8/9 in compressible

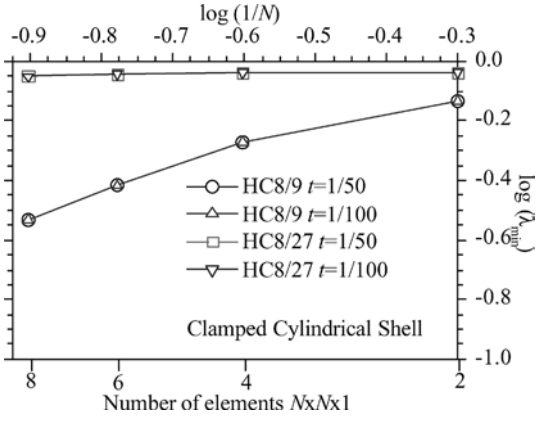

Fig. 4. Clamped cylinder: inf–sup values

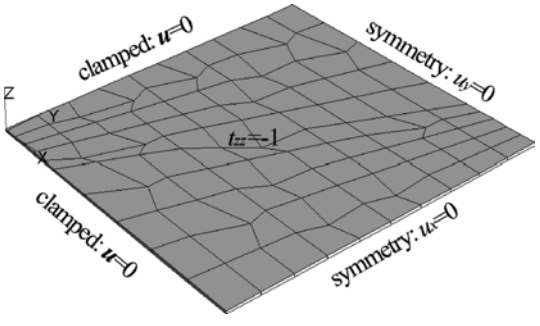

Fig. 5. The plate bending model problem

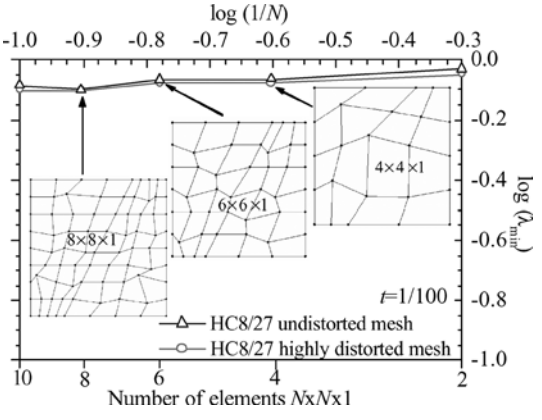

Fig. 6. Clamped plate: inf–sup test

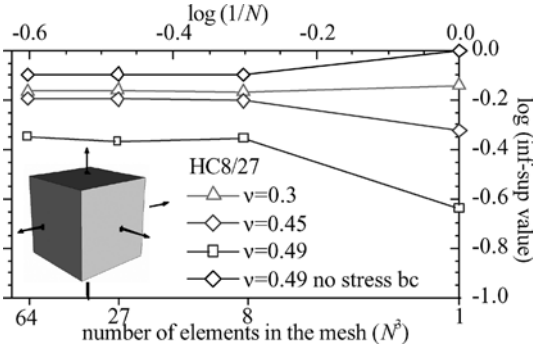

Fig. 7. Unit brick: inf–sup values

cases and HC8/27 in nearly incompressible case. The considered models are isotropic or orthotropic, although present formulation allows analysis of anisotropic materials. In addition, present formulation allows introduction of initial strains, beside before mentioned initial displacements and initial stresses. Nevertheless, cases where material is anisotropic and/or where initial strains are prescribed, are left for the further report.

It should be emphasised that target results for the popular plate/shell benchmarks tests, are usually obtained by the some plate/shell theory based on dimensional reduction in the direction normal to middle surface. Therefore, the difference between results obtained by the present full theory, in accordance to available target values, is expected. The visualisation of results is provided by the Straus7 software package [22] or by the *in-house* software package.

6.1
Model problem with singularity

One of the serious complaints to the mixed formulations is that they result with unrealistic oscillation around theoretical solution in the presence of the singularity caused by the nonsmoothness of data (such as jump boundary conditions or singular loads) or the nonsmoothness of the solution domain (such as corners or cracks). To examine sensitiveness of the present finite element to the nonsmoothness of the solution domain, the popular L-shaped model problem [23] shown in Fig. 8, is considered.

Only a quarter of the present model problem is analysed due to the symmetry. The stress distribution along the line BC that contains stress singular corner point S, is examined.

The stress distribution of the stress component t^{xx} along the line BC is shown in Fig. 9, where we may see that approximation by the finite element HC8/9 results with spurious stress oscillation. On the other hand, if we enrich approximation by enforcing the all six stress degrees of freedom at the mid-side (hierarchic) finite element nodes along the physical boundaries BS and AS only, calculated stresses are smooth. That case is denoted by the HC8/27, although only some of its nodes are utilized. Therefore, despite forced continuity of stress approximation functions in singular point S, we obtain expected non-oscillating stress distribution, for difference to the other mixed schemes (see [23], p. 363).

6.2
Cylindrical shell (“Scordelis-Lo” Roof)

A well known “Scordelis-Lo” Roof model problem shown in Fig. 10, subjected to gravity loading [24], is analysed. The specific weight is $\gamma = 0.20626$. The Young's modulus is $E = 4.32 \cdot 10^8$ and Poisson's ratio is $\nu = 0$. The cylindrical shell is simple supported on rigid diaphragms and free on the other sides. The advantage of the present model problem is that there are no singularities involved. There are two different values reported in the literature, 0.3024 [25] and 0.3086 [24].

The convergence of the displacement at the midpoint D on the free edge NA using HC8/9 finite element, is examined. The results were compared with finite element DSG4, bilinear four-nodded finite element based on the *Discrete Shear Gap* finite element method [25], which utilizes only displacement and rotational degrees of freedom at the nodes. It is wel-known for its explicit satisfaction of the kinematic equation for the shear strains at discrete points in order to effectively eliminate the parasitic shear strains. However, it was primarily chosen because no additional efforts have been made to improve its behavior, like in the case of the present finite element HC8/9.

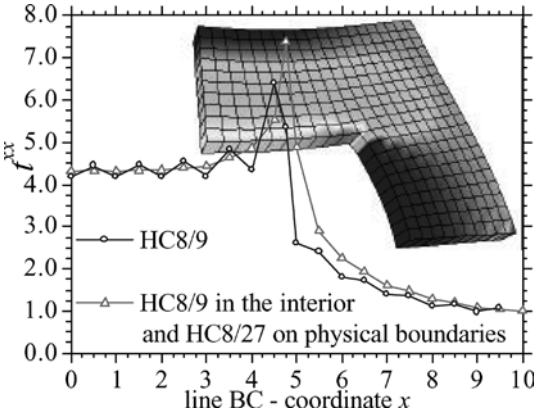

Fig. 9. L-shaped finite element model: stress distribution on line BC

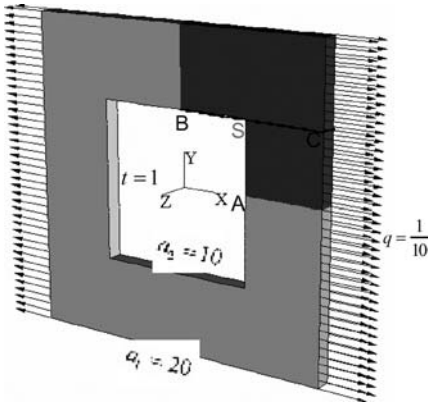

Fig. 8. L-shaped problem

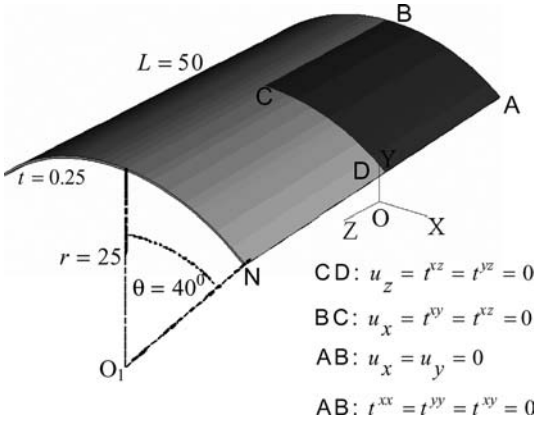

Fig. 10. “Scordelis-Lo” roof model problem

Only one-quarter of the starting model is analysed due to the symmetry. The own weight of the present shell is simulated by the uniform pressure $p = -90$. Displacement and stress boundary conditions are applied as shown in Fig. 10. The increasing sequence of HC8/9 finite element meshes, are analysed.

The convergence of the target vertical displacements $u_y(\mathrm{D}^{\mathrm{up}})$, for the present scheme and DSG4 approach, is shown in Fig. 11.

6.3 Clamped square plate

As a test in bending dominated situations, the clamped square plate model problem, with edge length $a = 2$ and thickness $t = 0.01$, subjected to the uniform pressure $q = -100$, is considered. The Young's modulus is $E = 1.7472 \cdot 10^7$, and Poisson's ratio is $v = 0.3$. The analytical solution for the maximal deflection at the plate centre C calculated by the Kirchhoff's plate theory is $w = 1.26$ [26].

Only a quarter of the plate, shown in Fig. 12, was analysed due to the symmetry. The essential stress boundary conditions $t^{zz}|_{z=0.01} = -100$ are prescribed for the nodes lying on the upper surface of the plate. Further, clamped edges were simulated by zeroing degrees of freedom connected to the displacement $(u_x = u_y = u_z = 0)$ and transversal shear stress components $(t^{xz} = t^{yz} = 0)$. This case, denoted as the Case A, is shown in Fig. 12. If we want to simulate the *plate theory*, the additional assumptions that all transversal shear stress components (t^{xz} and t^{yz}) can be neglected (set to zero) must be utilised. That case is denoted as Case B.

The present model problem was discretized by the sequence of meshes with two layers of brick finite elements HC8/9 per thickness, that is $N \times N \times 2$. Therefore, axial dimension of the finite elements in the direction normal to the middle of the plate plane will be $(1/100)/2 = 0.005$. Consequently, in the case of the roughest $(N = 8)$ and finest finite element mesh $(N = 40)$, the ratio between minimal and maximal axial dimension in the solid brick finite element, will be $r = 0.125/0.005 = 25$ and $r = 0.025/0.005 = 5$, respectively.

The convergence of the transversal displacements at the plate centre for the cases A and B, is shown in Fig. 13. From the numerical result obtained by the present method in the case A, we may see that target results converge from below to the solution that is a little bit lower than one obtained by the Kirchhoff's plate theory. On the other hand, in the case B, where the assumptions of the plate theory were respected as much as possible, the target results for the sequence of refined meshes instantly converge to the solution which is a little bit less than one obtained by the Kirchhoff's plate theory. The possible explanation for that phenomenon is given in the next numerical example.

In Table 2, the absolute relative displacement error (η) in accordance to the target results, as well as the work of external forces (W), for both analysed cases are given.

The convergence of stress component t^{zz} at node A (see Fig. 12), for both analysed cases, is shown in Fig. 14.

From the present example, we may draw the conclusion that present approach is sensitive to the simulation of the stress boundary conditions. Therefore, its proper determination is of a great importance.

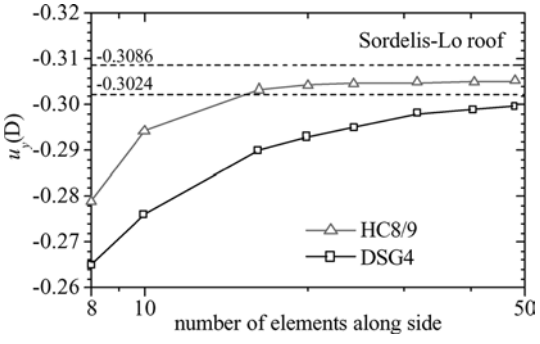

Fig. 11. "Scordelis-Lo" roof: maximal displacements

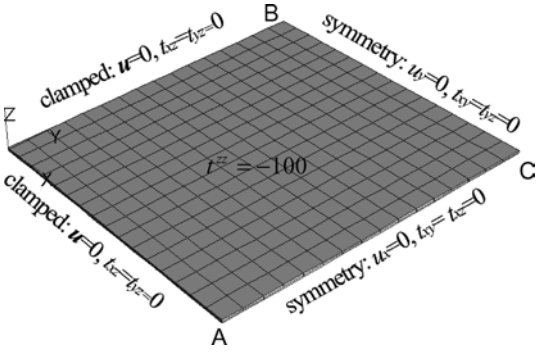

Fig. 12. Clamped plate finite element model – case A

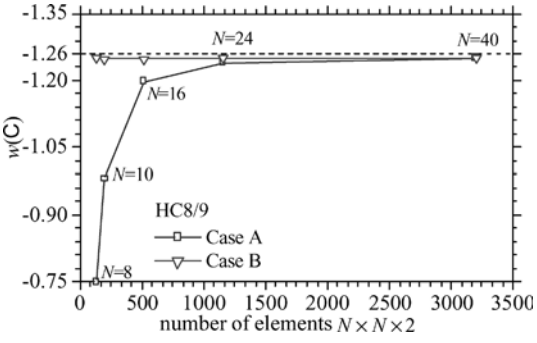

Fig. 13. Clamped square plate: maximal deflection

Table 2. Convergence: displacement error and work

Model	η (%)		W	
	Case A	Case B	Case A	Case B
8	40.5569	0.8249	10.14775	19.03642
10	22.1804	0.9085	13.71001	19.06954
16	4.9201	0.8971	17.86789	19.13062
24	1.5685	0.8111	18.91428	19.17450
40	0.7581	0.6971	19.19474	19.21678

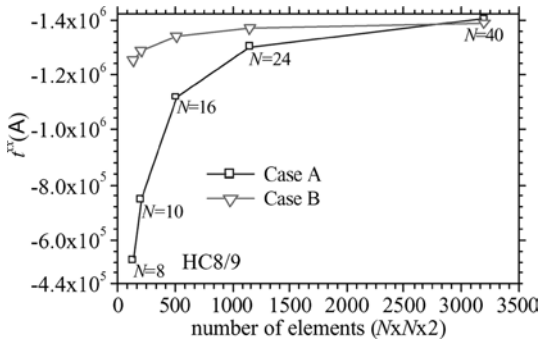

Fig. 14. Clamped square plate: maximal stress

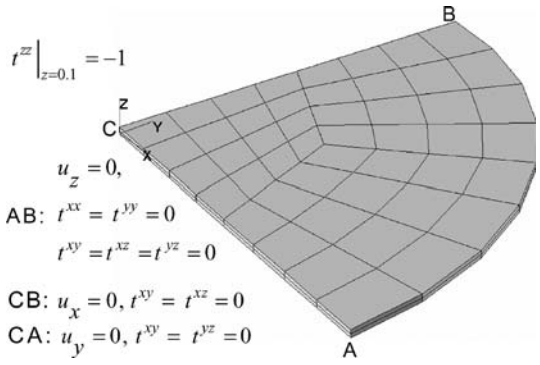

Fig. 15. Circular plate: boundary conditions

6.4
Simply supported circular plate

A clamped circular plate [27] under uniform normal pressure $p = 1$ shown in Fig. 15, is analyzed. The radius of the plate is $r = 5$ and thickness of the plate is $t = 0.1$. The material is isotropic, modulus of elasticity is $E = 1092000$ and Poisson's ratio is $\nu = 0.3$. The plate theory solution for the central displacement and maximal radial stress component in the centre of the plate are $w = -0.398137$ and $t^{rr} = 3093.75$ [26], respectively. The model problem has two planes of symmetry. Therefore, one-quarter is analysed, only. The resulting finite element mesh is distorted.

The present model problem is discretized by the two layers of brick finite elements HC8/9 per thickness, that is $N \times N \times 2$. The essential boundary conditions per displacements and stresses, for case A, are given in the Fig. 15. Hence, we will also examine case B, where degrees of freedom of transversal shear stress components are inactive (set to zero), as in the case of *plate theories*.

For comparison, the results are compared with the low order plate bending finite element with thickness change and enhanced strains, proposed by Piltner and Joseph in [27], which is derived from the three-dimensional variational formulation, where three-dimensional constitutive equation for six stress components has not to be modified. The considered two-dimensional meshes are discretized with a same pattern as present are (see Fig. 15).

In Fig. 16 we may see that both analysed cases (Case A and Case B), converge to the same value. Therefore, we may draw the conclusion that success of the Case B is mirage, from the reason that instant convergence is obtained on the account of the unrealistic neglecting of the transverse shear stress components. In other words, by minimizing shear stress influence (case B) we have "softened" the finite element mesh, so it may instantly undergo apparently higher deflections. This explains fast convergence of the considered plate element, also.

Nevertheless, maximal deflections of the sequence of finite element meshes approximated by the present finite element converge to the value that is a little bit lower than one obtained by the Kirchhoff's plate theory.

The convergence of the maximal stress values $t^{rr}(\mathrm{C})$ for the cases A and B, where central node C belongs to the lower surface of the considered model, is shown in Fig. 17. The numerical solutions are compared with target results obtained by the plate theory [26]. We may see that both

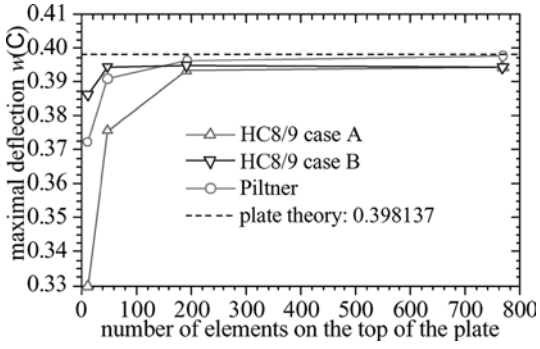

Fig. 16. Circular plate: maximal deflection

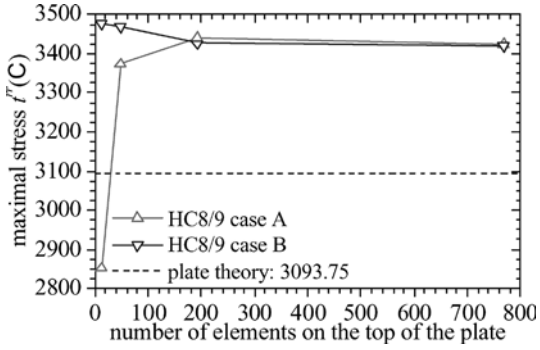

Fig. 17. Circular plate: maximal stress

cases converge to the same value that is about 10% in error to the theoretical result.

6.5
Twisted beam

The clamped thick twisted beam shown in Fig. 18, under in-plane and out-of-plane unit loading at its free end [28], is analysed. The dimensions of the untwisted beam are $12 \times 1.1 \times 0.32$. The beam is gradually twisted, so that its free end is rotated by 90° in accordance to its clamped end. The material is isotropic, modulus of elasticity is $E = 2.9 \cdot 10^7$ and Poisson's ratio is $\nu = 0.22$. The theoretical solution for the maximal displacement at the free end for the in-plane loading is $u_y(\mathrm{C}) = -5.426 \cdot 10^{-3}$, and for the out-of-plane loading is $u_x(\mathrm{C}) = -1.756 \cdot 10^{-3}$.

The beam is discretized using the increasing sequence of the meshes $N \times 4 \times 2$, where $N = 12, 16, 96$. Two cases

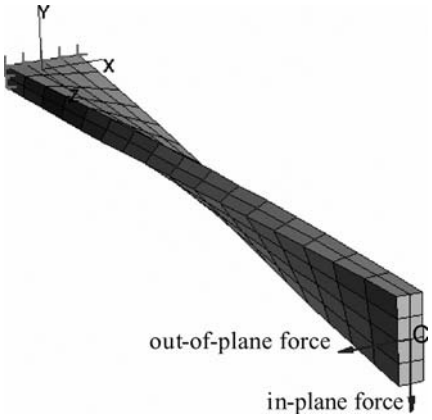

Fig. 18. Twisted beam

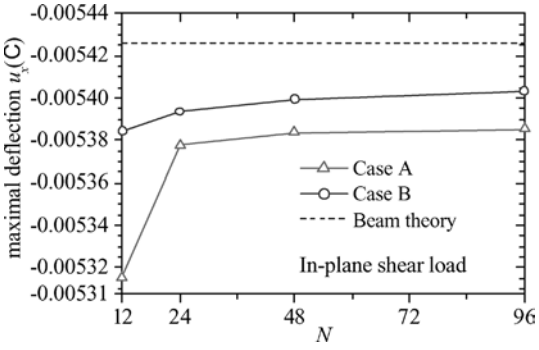

Fig. 19. Twisted beam: in-plane shear load

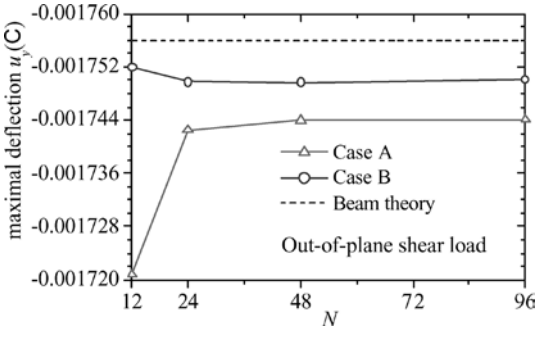

Fig. 20. Twisted beam: out-of-plane shear load

of boundary conditions per displacement and stresses are considered. Thus, boundary conditions for Case A are $\{z = 0 : u_x = u_y = u_z = t_{xy} = t_{xz} = t_{yz} = 0\}$, and for case B are $\{z = 0 : u_x = u_y = u_z = t_{xy} = t_{xz} = t_{yz} = 0\}$ and $\{\Omega \cup \partial\Omega : t_{xz} = t_{yz} = 0\}$. The results are plotted in Figs. 19 and 20.

Further, the absolute relative displacement error (η) of these solutions comparing to target one, as well as work of external forces (W), are given in Tables 3 and 4.

The visualization of the deformed model configuration and maximal stress component is given in Fig. 21.

From the results reported in Tables 3 and 4, we may see that present approach is less than 1% in error in accordance to the beam theory. Nevertheless, present author are of opinion that full approximation of stresses is recommended, regardless of little difference in accordance to the theory solution.

Table 3. Twisted beam: convergence for the in-plane loading

In-plane Model	η (%)		W	
	Case A	Case B	Case A	Case B
12	2.04	0.76705	2.6576E−3	2.6922E−3
24	0.89	0.59771	2.6889E−3	2.6968E−3
48	0.78	0.48749	2.6919E−3	2.6998E−3
96	0.75	0.41821	2.6927E−3	2.7017E−3

Table 4. Twisted beam: convergence for the out-of-plane loading

Out-of-plane Model	η (%)		W	
	Case A	Case B	Case A	Case B
12	2.01	0.22722	8.5782E−4	8.7601E−4
24	0.77	0.35752	8.7124E−4	8.7486E−4
48	0.69	0.35985	8.7196E−4	8.7484E−4
96	0.68	0.33747	8.7202E−4	8.7504E−4

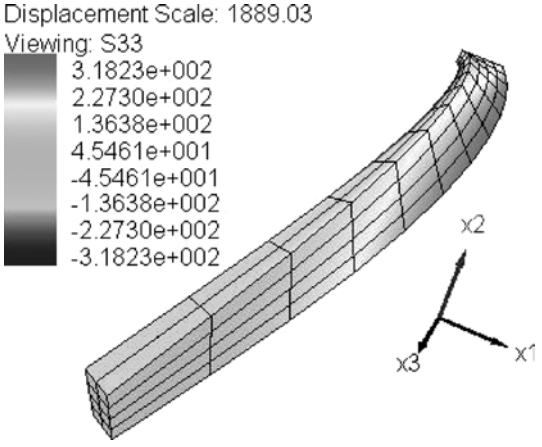

Fig. 21. Twisted beam out-of-plane loading: maximal stress result

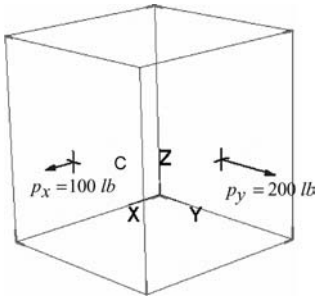

Fig. 22. Orthotropic solid: undeformed mesh

6.6
Stretching of an orthotropic solid

A cube of side $L = 1$ *in* subjected to distributed surface loads, is shown in Fig. 22. The material is assumed to be orthotropic and the material axes coincide with the global ones. Material data are: Young's moduli $E_1 = 10 \cdot 10^6 psi$, $E_2 = 20 \cdot 10^6 psi$, $E_3 = 40 \cdot 10^6 psi$, shear moduli

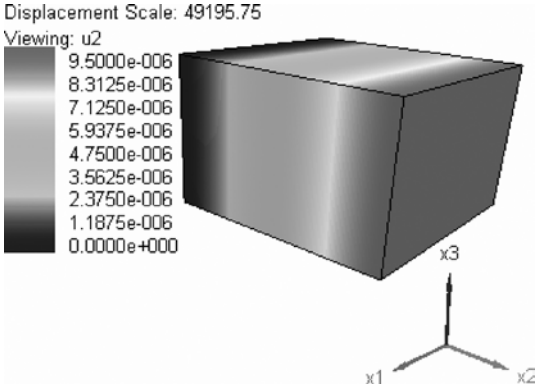

Fig. 23. Orthotropic solid: maximal displacement

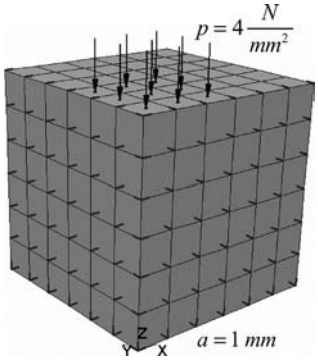

Fig. 24. Block under compression

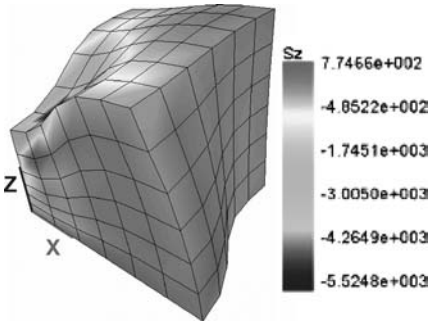

Fig. 25. Block under compression: maximal stresses

$G_{12} = G_{13} = G_{23} = 10 \cdot 10^6 psi$ and Poisson's ratios $N_{12} = 0.05$, $N_{23} = 0.1$, $N_{31} = 0.3$, where $N_{21} = (N_{12}E_2)/E_1$, $N_{32} = (N_{23}E_3)/E_2$ and $N_{13} = (N_{31}E_1)/E_3$. The target values are three displacements $\mathbf{u}(\mathrm{C}) = \{u_x, u_y; u_z\}$ components of point C, that is $\mathbf{u}(\mathrm{C}) = \{9, 9.5, -1.75\} \times 10^{-6} in$. As the cube is under constant strain deformation, we expect exact results even with only one finite element mesh. The results obtained coincide with exact.

The visualization of displacement component $u_y \equiv u_2$ is shown in Fig. 23.

6.7
Nearly incompressible block under compression

In the present example, we will test whether present finite element exhibits Poisson's effect (volumetric locking) in the limit of incompressibility allied to mesh distortion [29]. Brick under compression p_0 on the middle part of its two opposite surfaces, is analysed. One octant of the system is discretized due to the symmetry. Geometry, loading and boundary conditions of the system are described in Fig. 24, in which short line represents suppressed displacement along that direction. The nodes on the top of the structure are constrained in x and y direction. The material parameters are $\mu = 80.194$ N/mm^2 and $\lambda = 400889.806$ N/mm^2. Consequently, modulus of elasticity is $E = 240.56595979$ N/mm^2 and Poisson's ratio is $\nu = 0.499899987$.

The deformed configuration of the considered $6 \times 6 \times 6$ finite element HC8/27 mesh, superimposed with picture of the stress component t^{xx}, shown in Fig. 25, reveals that there is no spurious behaviour of displacement and stresses when the finite element HC8/27 is used.

7
Conclusions

The three-dimensional multifield finite element approach in elastostatics analysis of isotropic, orthotropic and anisotropic materials, based on Hellinger-Reissner's principle with no dimensional reduction and numerical tune-ups, for direct calculation of full stress (six independent components of second order stress tensor) and displacement (three components of displacement vector) fields, is presented. It has two essential contributions in accordance to the similar approaches, the stress field is approximated by continuous base functions, and known stress constraints may be treated as the essential boundary conditions. In addition, there is possibility to apply initial displacement and stress (or strain) field. It is proven that proposed finite element HC8/27 is reliable, even in the limit problems discretized by highly distorted meshes. Consequently, it could be recommended for the use in the analysis on non-smooth model problems of arbitrary geometry in the compressible and nearly incompressible limits. Accordingly, its restriction HC8/9, which does not pass inf–sup test is suggested for the analysis of regular model problems.

In order to avoid the geometrical invariance error and to enable introduction of known displacement and stress constraints and surface forces, in an adequate coordinate systems, the underlying finite element scheme is coordinate independent.

The satisfaction of convergence requirements of the present finite element scheme makes it a promising field for future research undertakings, including research in the materially non-linear solid continua. In addition, capability to introduce initial strain due to, for example, thermal effects makes the present approach applicable for determination of thermal stresses, which is left for further report.

References

1. **Arnold DN** (1990) Mixed finite element methods for elliptic problems. Comput. Meth. Appl. Mech. Eng. 82: 281–300
2. **Brezzi F, Fortin M, Marini D** (1993) Mixed finite element methods with continuous stresses. Math. Models Meth. Appl. Sci. 3(2): 275–287
3. **Bathe KJ, Iosilevich A, Chapelle D** (2000) An inf-sup test for shell finite elements. Comput. Struct. 75: 439–456

4. **Cao YP, Hu N, Lu J, Fukunaga H, Yao ZH** (2002) A 3D brick element based on Hu–Washizu variational principle for mesh distortion. Int. J. Num. Meth. Eng. 53: 2529–2548. DOI: 10.1002/nme.409
5. **Brezzi F, Fortin M** (1991) Mixed and hybrid finite element methods. Springer-Verlag, New York
6. **Berkovic M, Draškovic Z, Mijuca D** (1998) A direct block sparse solution of the mixed finite element equations. Comput. Assisted Mech. Eng. Sci. 5: 21–30
7. **Mijuca D, Berkovic M** (1998) On the efficiency of the primal-mixed finite element scheme. Adv. Comput. Struct. Mech. Civil-Comp Press, pp 61–69
8. **Bottasso CL, Borri M, Trainelli L** (2002) Geometric invariance. Comput. Mech. 29: 163–169. DOI 10.1007/s00466-002-0329-8
9. **Rannacher R, Suttmeier FT** (1997) A feed-back approach to error control in finite element methods: application to linear elasticity. Comput. Mech. 19(5): 434–446
10. **Robey TH** (1992) The primal mixed finite element method and the LBB condition. Numer. Meth. Partial Differential Equations 8: 357–379
11. **Bathe KJ** (2001) The inf-sup condition and its evaluation for mixed finite element methods. Comput. Struct. 79: 243–252
12. **Mirza FA, Olson MD** (1980) The mixed finite element in plane elasticity. Int. J. Numer. Meth. Eng. 15: 273–289
13. **Berkovic M, Draškovic Z** (1991) On the essential mechanical boundary conditions in two-field finite element approximations. Comput. Meth. Appl. Mech. Eng. 91: 1339–1355
14. **Zienkiewicz OC, Zhu JZ, Taylor RL, Nakazawa S** (1986) The patch test for mixed formulations. Int. J. Numer. Meth. Eng. 23: 1873–1883
15. **Berkovic M, Draškovic Z** (1994) A two-field finite element model related to the Reissner's principle. Theor. Appl. Mech. 20: 17–36
16. **Berkovic M, Mijuca D** (1999) On the main properties of the primal-mixed finite element formulation. Facta Universitatis Series Mechanics, Automatic Control and Robotics. 2(9): 903–920
17. **Mijuca D** (2002) A new reliable 3D finite element in elasticity. In: Proceedings of the fifth world congress on computational mechanics (WCCM V), Mang HA, Rammerstorfer FG, Eberhardsteiner J (eds) Vienna University of Technology, Austria
18. **Oden JT** (1972) Finite elements of nonlinear continua. McGraw-Hill, New York
19. **Axelsson O, Barker VA** (1984) Finite element solution of boundary value problem. Academic Press, Inc
20. **Olson MD** (1983) The mixed finite element method in elasticity and elastic contact problems. In: Atluri SN, Gallagher RH, Zienkiewicz OC (eds) Hybrid and mixed finite element methods, John Wiley & Sons, pp 19–49
21. **Kasper EP, Taylor RL** (1997) A mixed-enhanced strain method: linear problems. University of California, Report No.UCB/SEMM-97/02
22. **G+DComputing**, Straus7, Finite element analysis system software package, www.strand.aust.com, Australia
23. **Zienkiewicz OC, Taylor RL** (1989) The finite element method. Vol I. McGraw-Hill, London
24. **Scordelis AC, Lo KS** (1964) Computer analysis in cylindrical shells. J. Am. Concrete Institute 61: 561–593
25. **Bletzinger KU, Bischoff M, Ramm E** (2000) A unified approach for shear-locking-free triangular and rectangular shell finite elements. Comput. Struct. 75: 321–334
26. **Timoshenko S, Goodier JN** (1970) Theory of elasticity. McGraw-Hill, New York
27. **Piltner R, Joseph DS** (2001) An accurate low order plate bending element with thickness change and enhanced strains. Comput. Mech. 27: 353–359
28. **MacNeal RH, Harder RL** (1985) A proposed standard set of problems to test finite element accuracy. Finite Elements in Analysis and Design 1: 3–20
29. **Reese S, Wriggers P, Reddy BD** (2000) A new locking-free brick element technique for large deformation problems in elasticity. Comput. Struct. 75: 291–304